

Total hydrocarbon volume in place: improved reservoir characterization from integration of towed-streamer EM and dual-sensor broadband seismic data

Zhijun Du^{1*}, Ghazwan Namo², Joshua May¹, Cyrille Reiser¹ and Jonathan Midgley¹ present a geophysical reservoir characterization workflow that seeks to integrate elastic and electric attributes derived from inversion of seismic and CSEM data.

Introduction

Understanding reservoir characteristics, such as porosity, water saturation, thickness and the lateral extension of the reservoir is key for the characterization of a reservoir. These parameters are important because they serve as veritable inputs for reservoir volumetric analysis, i.e. estimating the total volume of hydrocarbon in place. Seismic data provide high-resolution images of the subsurface structure, but attempts to map fluids from seismic data may be misleading due to the ambiguity between lithology-fluid and lithology effects. In contrast, CSEM (Controlled Source Electromagnetic) data constrains subsurface resistivity – a physical property that strongly correlates with the fluid content and saturation of hydrocarbon reservoirs. By carefully integrating complementary information from both types of data, the limitations of each method can be overcome and the strength of each exploited. Used together, they help to better understand the prospect and the reservoirs characteristics, ultimately de-risking exploration, and the further applications in field development and reservoir management.

Rock physics models are transforms used to convert rock and fluid descriptions into geophysical properties such as resistivity or elastic moduli. The integration of seismic and CSEM data

requires a reliable and robust rock physics framework. CSEM data analysis can now be integrated into reservoir characterization workflows, particularly in areas where the geophysical understanding is ambiguous when using a conventional seismic reservoir characterization approach. Among the applications, the integration of pre-stack seismic inversion attributes with CSEM attributes using a rock physics framework constitutes one of the most modern and robust methodologies in geophysical reservoir characterization (see Harris et al., 2009; Gao et al., 2012; Pedro et al., 2017). Such an approach provides, in many circumstances, the most effective way of addressing the challenges of the complexities involved in data integration. However, due to the fact that the relationship between reservoir parameters and the corresponding elastic and electrical properties is non-unique and subject to uncertainties, and that the sensitivities of seismic and electromagnetic data are quite different, two major approaches have been adopted in reservoir characterization: (1) full quantitative joint inversion of seismic and CSEM data (for example Du and MacGregor, 2010; Chen and Hoverston, 2012;), albeit under development in application to geologically complex areas; (2) an approach based upon a staged quantitative integrated

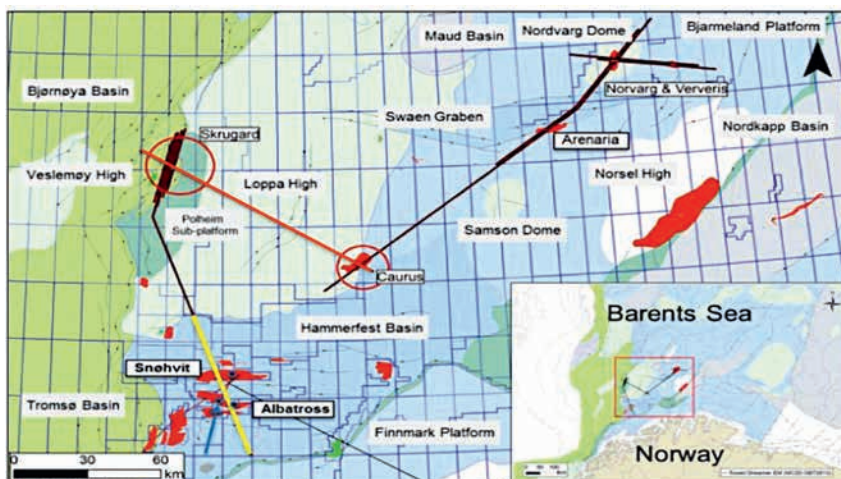


Figure 1 An overview of Johan Casberg area in the Barents Sea. The coloured lines indicate the collocation of the dual-sensor seismic and towed-streamer EM 2013 survey, where the thick red line indicates Line BS034 over Skrugard.

¹ PGS | ² Formerly of PGS

* Corresponding author, E-mail: Zhijun.du@pgs.com

interpretation workflow that seeks to integrate elastic and electric attributes derived from inversion of seismic and CSEM data, respectively, provides a very effective way of utilizing their complementary information.

In this paper we present a geophysical reservoir characterization workflow in which the latter integration approach is adopted. The characterization workflow allows the seismic, well log and towed-streamer EM technologies to make selective contributions according to their strengths. The workflow was successfully applied to a number of reservoir characterization projects and we present here an application to Skrugard, one of the most recent discoveries in area of the Johan Castberg, located in the geologically complex Barents Sea. The use of data integration enables reservoir characterization to discriminate between lithology and fluid properties, and to discern hydrocarbon from brine-saturated sands. We image the spatial distribution of the hydrocarbon volume (HCV) within the reservoir unit, which thus leads to quantitative estimates of the total volume of hydrocarbon in place within the reservoir.

The Johan Castberg area, Barents Sea

The discovery of the Skrugard reservoir (which now together with the Havis and Drivis discovery is called Johan Castberg) was a major milestone in the exploration of the Barents Sea (Figure 1). The area of interest covers the Hammerfest Basin, Loppa

High and the Polheim subplatform. The Skrugard discovery is located within the Bjørnøyrenna Fault Complex on the crest of a partly eroded north–south-trending rotated fault block. A combination of structural tilting of the Realgrunnen Subgroup reservoirs containing the Stø, Nordmela and Tubåen formations, and truncation of the intra-Cretaceous unconformities at the crest of the fault block, has formed the Skrugard trap (Figure 2). The structural apex is at 1204 m below MSL, and the elongated four-way closure covers an area of ~14 km². The water depth in the area is ~370 m. The appraisal well 7220/5-1 was drilled in 2012 and encountered both gas and oil. The reservoir zone interval containing hydrocarbons was ~100 m thick in most of the structure.

Towed-streamer EM

The PGS towed-streamer EM system described here consists of a towed source and EM streamer which are both towed from a single vessel. It was designed to enable efficient acquisition of CSEM data together with seismic data. The EM source consists of an 800 m long horizontal electric dipole (HED) towed at 10 m below the sea surface. The source signal is in the form of an optimized repeated sequence (ORS) generated by an oscillating current of +/- 1500 A. The distribution of source energy was designed within a usable frequency range of two decades spanning 0.1-10 Hz. The streamer has 72 electric field

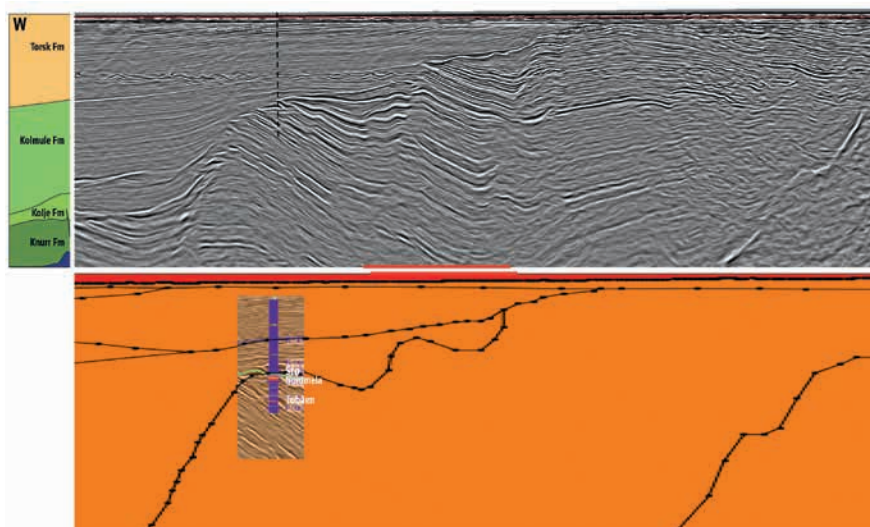
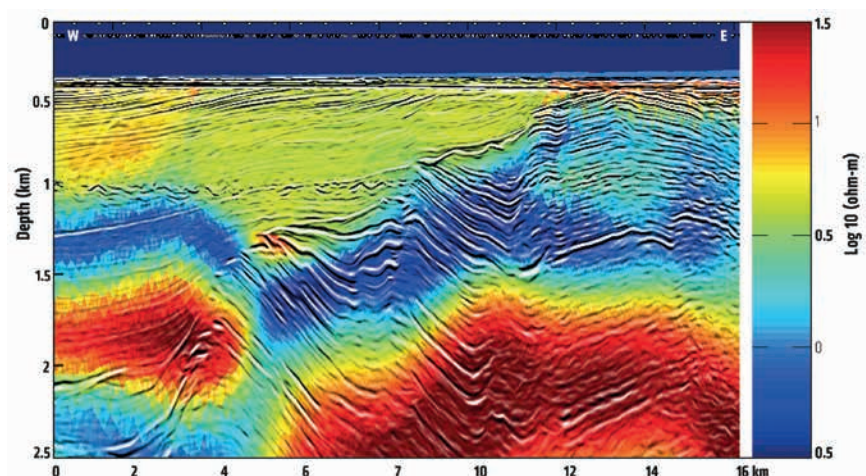


Figure 2 An illustrative set-up for conducting seismically guided inversion for Line BS034. The upper panel shows the coincident broadband dual-sensor seismic section in depth, and the lower panel shows the interpreted seismic horizons extracted for guiding the inversion.

Figure 3 The results of the 2.5D seismically guided anisotropic inversion for Line BS034. The vertical resistivity is co-rendered with the depth converted seismic sections.



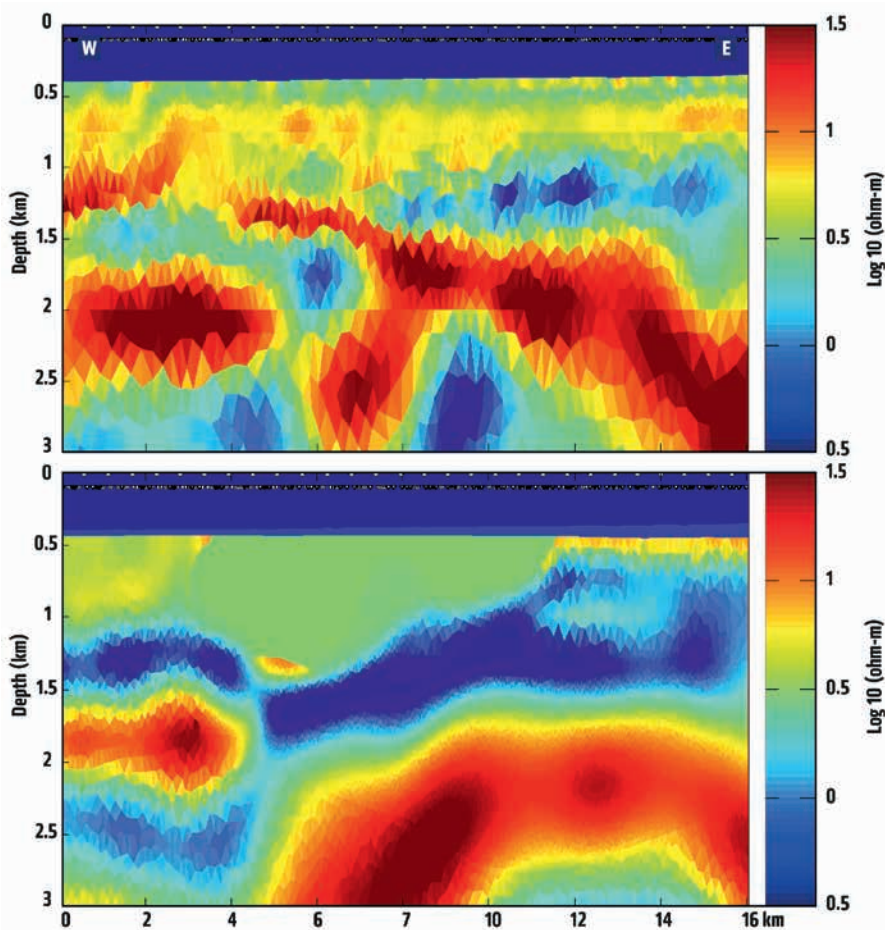


Figure 4 Comparison of two vertical resistivity models derived from the unconstrained (upper panel) and seismically guided (lower panel) inversion for the Line BS034.

channels consisting of electrode pairs effectively providing up to 72 offsets, from 0-7700 m relative to the centre of source, with an average offset interval of ~160 m over the offset ranges. The towed-streamer EM system thus provides the dense sampling, data quality, and signal-to-noise ratio required for imaging challenging targets embedded in the complex geological environment under a shallow sea water column.

Unconstrained and seismic guided EM inversion

In this study, the survey line BS034 (the thick red line in Figure 1) was used and represents a sub-dataset from the PGS 2013 Towed Streamer EM survey acquired over Johan Castberg, in the Barents Sea. Line BS034 crosses the short axis of the Skrugard discovery (about 2 km wide); over the surface location of the well 7220/5-1 and approximately perpendicular to the geological strike direction. The BS034 dataset consists of six frequencies: 0.2, 0.8, 1, 1.4, 2.2 and 2.6 Hz.

Unconstrained Inversion

We used regularized anisotropic 2.5D inversion to recover the sub-surface resistivity. The inversion code used is MARE2DEM. The forward modelling kernel of MARE2DEM is based on the adaptive finite element code of Key and Owall (2011), and the inversion scheme is based on the ‘Occam’ inversion of Constable et al. (1987), a regularized variant of Gauss-Newton minimization. In general, it was found that anisotropic inversion is required when inverting towed-streamer EM data in the Barents Sea due to significant anisotropic background structures. Without using ani-

sotropic inversion the resistivity sections were banded with high contrast layers as an artifact of effective anisotropy, apparently representing no plausible geological scenario, and were created by enforcing an isotropic structure (Key et al., 2014).

The unconstrained inversion forms the first step of our staged towed-streamer EM data processing and inversion workflow. We use unconstrained inversion to seek the best model that fits the data, which is the smoothest model in the first derivative sense (Constable et al., 1987). Although unconstrained inversion takes no account of complex or higher dimensional structures, it allows the class of structures to which the data are the most sensitive, and the variations in these structures to be assessed.

Seismically Guided Inversion

We have developed a workflow to make the inversion-based EM process more data and information-driven. The design of the workflow utilizes the advantages of the two high fidelity datasets: dual-sensor broadband seismic and towed-streamer EM. The seismically guided EM inversion described in Du and Hosseinzadeh (2014) facilitates an optimal procedure to combine the complementary information from seismic and EM data, with the seismic data optimally for constraining structure, and the EM data optimally for constraining resistivity.

For line BS034, seismically guided EM inversion was initialized by a starting model through the integration of resistivity information from unconstrained inversion with the interpretation of the dual-sensor seismic data. The starting model is divided into a number of regions/blocks (Figure 2) by seismically constrained

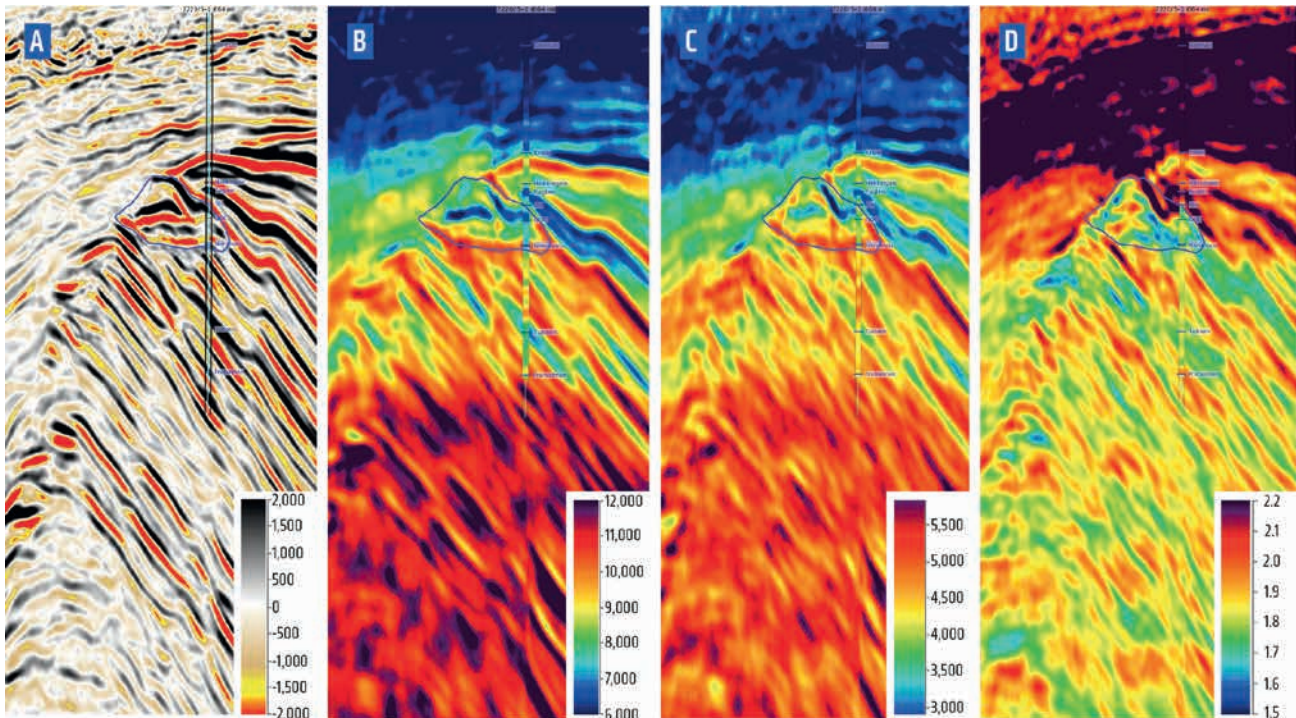


Figure 5 Line BS034 seismic data: (a) Near angle stack, (b), P-wave impedance (I_p), (c), S-wave impedance (I_s), and (d) V_p/V_s , all with the corresponding 7220/5-1 logs superimposed. The black polygon identifies the reservoir. In the P-wave impedance the intra-reservoir shales appear yellow-red while the gas/oil sands are blue-green.

geological horizons, including Kolmule and Stø in the shallow part. The Kolmule Formation is marked by a sharp contact with the overlying Torsk Formation of late Paleogene age. The Stø Formation at the well location, consists of ~80 m clean sand and has good reservoir seismic properties. The reservoir encountered in well 7220/5-1 consists of the Stø, Nordmela and Tubåen formations, overlaying by Fuglen shale (reservoir seal) (Figure 2). The resistivity in each region above Stø was set by the plausible lower and upper boundaries that are the lowest and highest average anisotropic resistivities, constrained by the preceding unconstrained inversions. The remaining regions (below Stø) of the model were all set as parameter-free space for the inversion.

Figure 3 shows the seismically guided anisotropic inversion for Line BS034 (For brevity horizontal resistivities are not shown). The benefits of incorporating seismic data into the inversion are evident when comparing the unconstrained and seismically guided 2.5D inverted vertical resistivities in the upper and lower panels of Figure 4, respectively. The unconstrained inversion has successfully recovered the background resistive structures (upper panel of Figure 4), but some spurious distributed resistors extended to a depth of ~1.3 km in the west and to about 0.7 km in the east. In contrast, the lower panel of Figure 4 shows that the seismically guided inversion shows a more homogeneous layer after smoothing the spurious features arising from the unconstrained inversion. A good correlation between acoustic and electromagnetic features is observable, where the shallow resistivity distributions are laterally following the strong seismic reflections (refer to Figure 3). Comparison of the upper and lower panels in Figure 4 reveals good consistency between the two results for the deeper part of the model, consisting of a large dumbbell-shaped resistive body (around 2 km depth) in the west part and a regional resistivity trend that crosses the middle and eastern part of the model.

Figure 3 shows that the seismically guided inversion successfully recovers the Skrugard reservoir, where a prominent high resistivity anomaly is spatially coincident with the geometry of the reservoir as constrained by the seismic data. By comparison to the most recently published model of the Skrugard 3D anisotropic inversion (Losest et al. 2014), we see that our model has significantly higher resolution and has recovered a more accurate (higher) resistivity value for restoring the reservoir strength. We believe this is mainly due to the fact that our inversion was conducted from a denser CSEM dataset. This is also demonstrated in Figure 7 (right panel) where the inverted resistivity at the Skrugard well 7220/5-1 location is accurately matching both top reservoir and the oil-water-contact (OWC), benchmarked by the log values. Such a high seismic-resolution EM image (Figure 3) also demonstrates the power of the data integration, resulting from fully utilizing the complementary information contained in the two high fidelity datasets.

Pre-stack seismic inversion

The seismic data for Line BS034 is shown in Figure 5 and was acquired concurrently with the EM data in 2013. The seismic datasets are good quality with high signal-to-noise (S/N) ratio. Compared to traditional seismic data, the broadband data give useable frequencies from as low as 2.5 Hz, and up to 200 Hz or higher for shallow targets, resulting in sharper seismic events with significantly reduced side lobe artefacts. Furthermore, the ultra-low frequencies reduce the use of well log information when building the low-frequency model (LFM) for seismic inversion (Reiser et al., 2015).

The pre-stack seismic data of Line BS034 have a broad bandwidth from 3 Hz to 60-70 Hz at the reservoir level, with good S/N ratio from near to far offsets. Four angle stacks were

created by stacking over the range of incident angles 5-15°, 15-25°, 25-35° and 35-45°. To gain insight into the reservoir lithology and fluid properties, inversion for both acoustic and shear (P and S) impedances is required. In addition, the low frequency information is also required for the computation of absolute elastic properties. By combining the low frequency model (LFM) with the seismic inversion, an estimate of the absolute elastic properties can be derived from the seismic data. A smooth background model in the 0-3 Hz range was thus constructed by kriging the well 7220/5-1 log data with the dual-sensor seismic velocity and constrained by the interpreted horizons. Pre-stack seismic inversion simultaneously inverted for P- and S-impedance.

Figure 5 shows the absolute P- and S-impedance results plus the estimated Vp/Vs volume. Both P and S impedance results delimit the reservoir and the flat spot, and the thicker intra-reservoir shales are well defined in the P-wave impedance, whereas the higher value of Vp/Vs delineates the Fuglen shale

(the reservoir seal). Note that Vp/Vs provides an additional tool to identify the main shale units, which were thereafter excluded from the calibration. This data example demonstrates the advantages of using dual-sensor broadband data for reliably retrieving the reservoir elastic properties with very limited well control.

Rock physics models

Geophysical properties of rocks, such as resistivity and elastic moduli, depend on mineralogy, pore fluid properties, and the geometry or fabric of the rock. An integrated interpretation approach relies on the successful derivation of a consistent rock physics framework that links geophysical properties to the rock and fluid description. Specifically, the task requires building the transform between in situ reservoir properties and quantities extracted from seismic and electromagnetic data, and whether the obtained transform built from well log-derived elastic and electrical attributes could posteriorly be applied field wide.

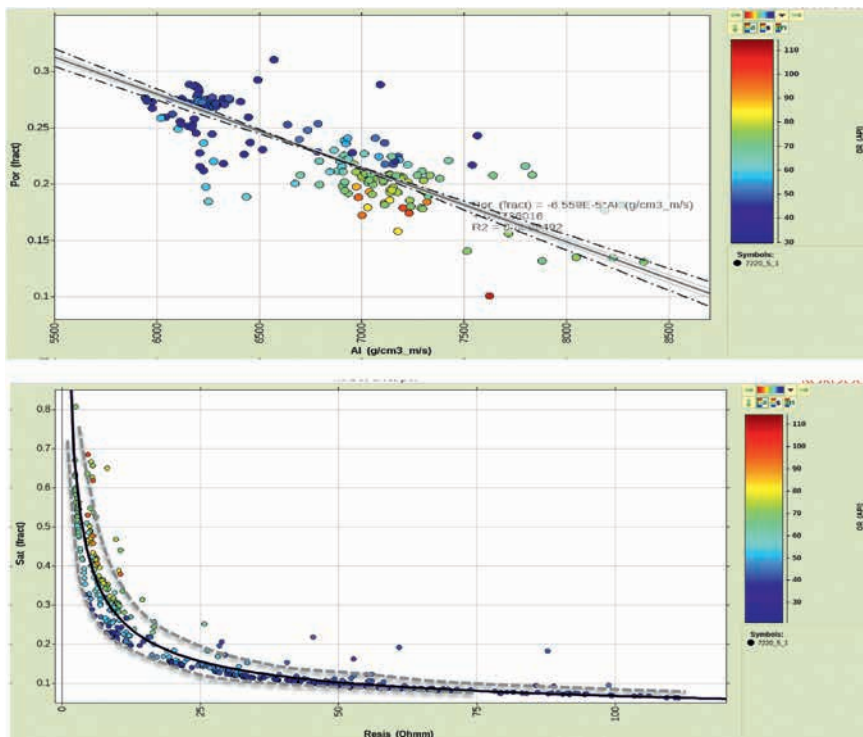


Figure 6 (upper) Cross-plot of Well 7220/5-1, porosity versus P-wave impedance for the reservoir sand, with the dashed lines defining the 95% regression confidence interval; (lower) Water saturation versus resistivity, with upper and lower bounds on saturation determined from the point cloud.

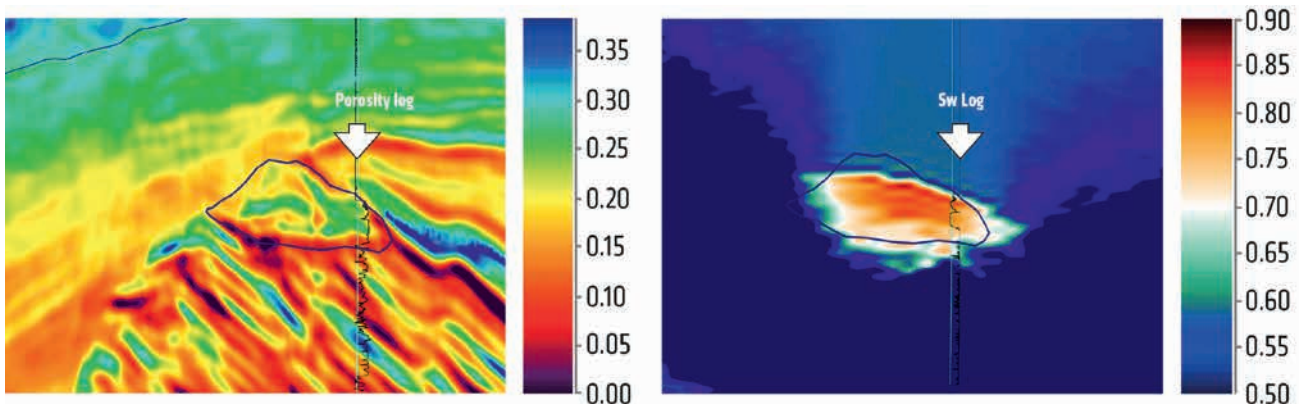


Figure 7 (left) Porosity volume estimation from P-wave impedance with log overlay; (right) hydrocarbon saturation volume estimation from the inverted vertical resistivity, with the water saturation log superimposed.

We started from well 7220/5-1, which was used to construct and validate acoustic and electric rock physics models for the Skrugard field. This process serves as a feasibility check, and along with well-ties, forms the first stage of our data integration workflow for extracting reservoir fluid properties. In the next stage the final results of acoustic impedance inversion and resistivity of EM inversion were extracted along well trajectories and compared to well log data to ensure the field model is consistent with the in-situ measurement. We then conducted realistic rock physics modelling by varying the fluid content and lithology (particularly shale content) to investigate the sensitivity of the surface data to these quantities. The modelling process thus acts as an additional QC procedure to help us understand whether ambiguities are resolved or remain unresolved by combining elastic and electrical data. In addition, the modelling process also provided the baseline for us to quantitatively assess the uncertainties in our final data integration products.

In Figure 6 we display the main results of the petrophysical evaluation and rock physics analysis from well 7220/5-1. It is observed that the linear correlation between P-wave impedance

and porosity in the reservoir interval was relatively high and shows a correlation of 0.85 (top panel of Figure 6). Upscaling these results with a running Backus average of velocities and density over a 10 m interval, and then using an arithmetic running average of porosity, produces a small change in the linear relationship. Thus, we feel confident in using the direct linear transform. We account for the ~15% of residuals (most likely to be the influence of clay within reservoir units) from the determined mean by defining the 95% regression confidence interval as the lower and upper variation bounds of the impedance-porosity transfer (top panel of Figure 6). We also observe that the relationship between resistivity and water saturation is quasi-exponential, which demonstrates the physics of rapidly decreasing resistivity with increasing water saturation (lower panel of Figure 6). Moreover, the relationship between the resistivity and water saturation is further complicated by the presence of the non-resolvable shales in the reservoir. This contributes to the uncertainty in hydrocarbon saturation estimates from the inverted EM resistivity. We therefore also produced the upper and lower bounds for the resistivity-

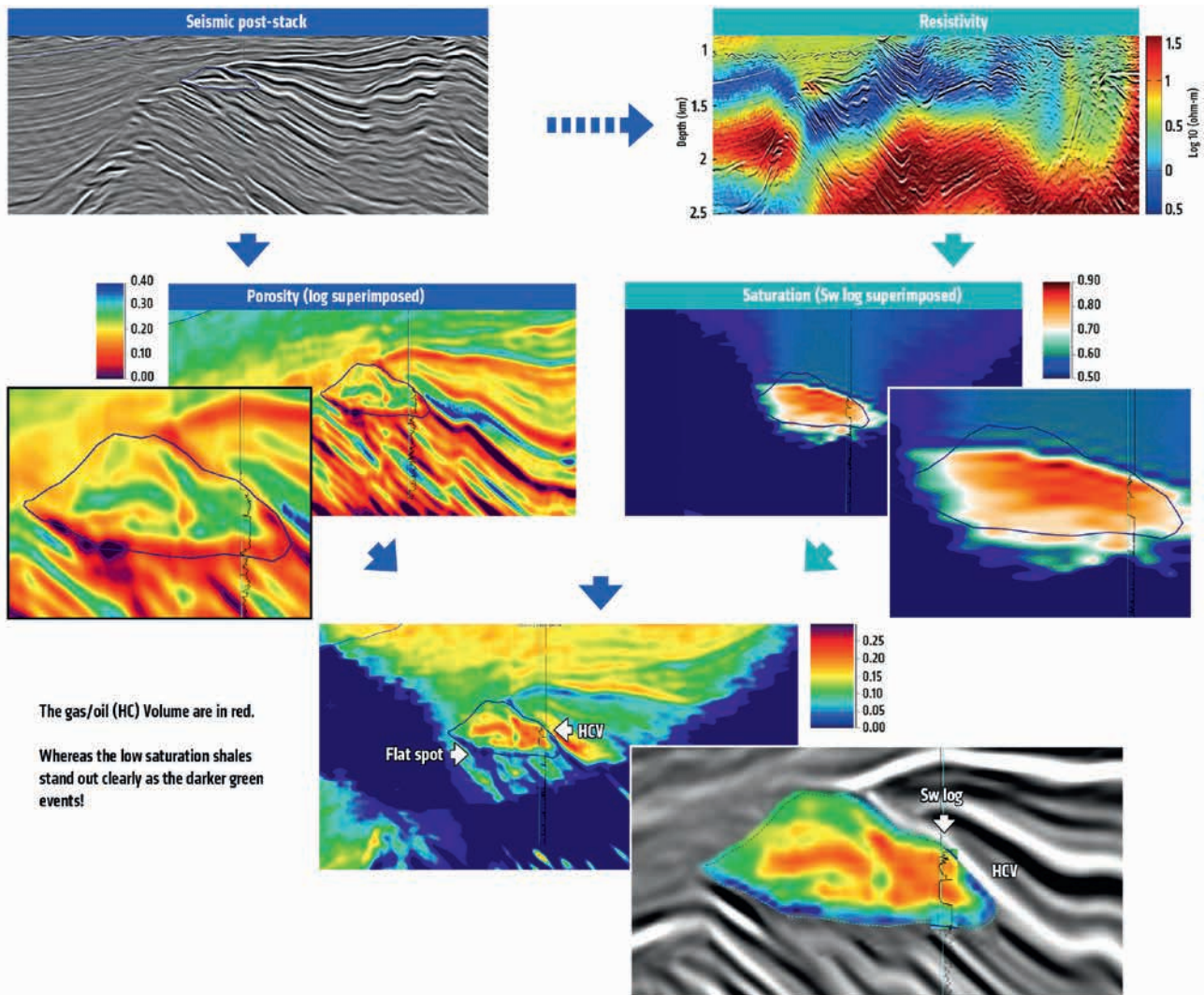


Figure 8 Schematic workflow for pursuing reservoir characterization from integration of seismic and CSEM data to map the fluid distribution within the reservoir. The final product is the hydrocarbon volume (HCV) display (lower panel). The low saturation shales stand out clearly as the darker green events, whereas the spatial distribution of HC volumes (indicated by the red colour) follows the complex reservoir filled faults blocks.

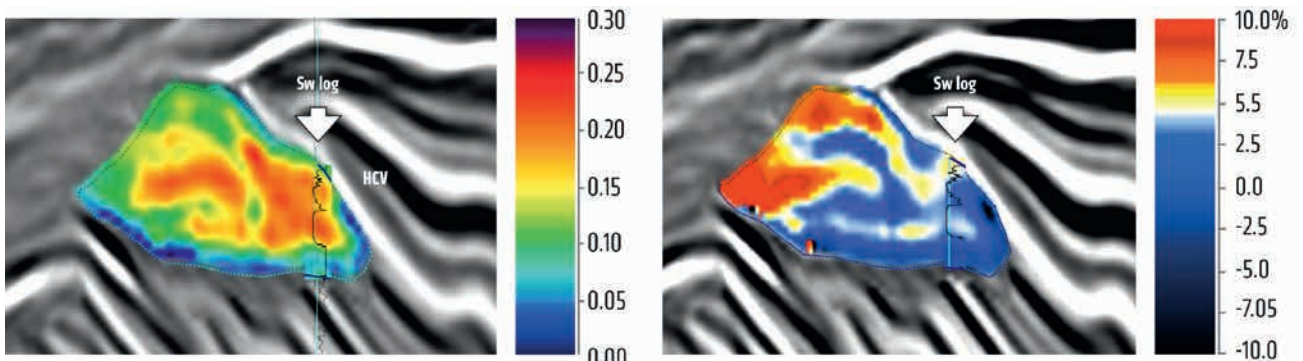


Figure 9 (left) The hydrocarbon volume (HCV) section derived from the data integration of CSEM and seismic inversions (ref. Figure 8) with the Sw log (well 7220/5-1) overlaid for comparison; (right) the uncertainties of HCV estimation from the rock physics integration (refer to the text for details).

saturation transfer from the cloud of the cross-plot (lower panel of Figure 6). As these data include the shale influence, the bounds are considered reliable, which provided us with a feasible way to assess uncertainties in the estimation of the hydrocarbon volume (HCV) within a reservoir. We will discuss this in some detail in the next section.

Data integration

The results of applying the rock physics models obtained from the well data, to reservoir rock fluid property estimates away from wells for the field, are shown in Figure 7. The porosity is obtained from the acoustic impedance, whereas hydrocarbon saturation is obtained from the resistivity. At the well location, a high correlation between field estimation and the in-situ well measurements is observed. Notice the excellent matches to the well log-derived rock properties demonstrating that both porosity and saturation were correctly predicted. It is further noted that it is unusual to get such an excellent surface-to-well tie from CSEM data, i.e., a very high correlation between well-measured water saturation to hydrocarbon saturation derived from the EM inverted resistivity model (right panel of Figure 7).

The lower panel of Figure 8 shows the combined result - a hydrocarbon-charged volume (HCV) display, i.e. the product of porosity and saturation (Harris et al. 2009). The HCV is a clearer indicator of the structures of the gas/oil spatial distribution. It shows that the high accumulation of hydrocarbon follows the complex Skrugard structural faulting (titled faults blocks). The image clearly delineates the sand and shale formations, where the intra-reservoir shales stand out as the darker green (see also the left panel of Figure 9). It highlights the relevant geological features and field architecture, differentiates sands and also the shale layer forming the reservoir seal. This case study demonstrates that we are now able to recover reservoir lithology and fluid information at the seismic-resolution scale through the data integration.

The right-hand panel of Figure 9 displays the uncertainties of the estimation of the HCV due to rock physics solution ambiguities as defined by the lower and upper bounds of the impedance-porosity transforms and resistivity-saturation conversions, respectively (Figure 6). Although the HCV uncertainties here are only obtained by statistically measuring the derivations from their relevant mean values, they are the true reflection of the complex relationship between the reservoir rock properties and the measurable earth

geophysical properties. A more accurate HCV map and associated uncertainties could be obtained by using a Bayesian framework, which is still under development (e.g. Figueiredo et al., 2017). Nevertheless, we have achieved a good structural conformance between the in-situ and the field data. Apparently, when applying to a large area with a potential increase geological complexity, the rock physics modelling approach adopted here would need to be extended to account for field spatial variation in rock properties. With regards to this and as shown in the right-hand panel of Figure 9, due to lateral variation of the reservoir property across the field, the uncertainties of the HCV become higher away from the well location, which is as expected.

Conclusions

The geophysical reservoir characterization workflow presented in this study demonstrates enhanced value through the uplift of sensitivity to changes in geophysical, rock and fluid properties in the subsurface. We quantified the benefit of data integration using an example based on the Skrugard (Johan Castberg) field in the Barents Sea.

The integration of multi-source geophysical data is not straightforward and has a number of technical challenges. Successful data integration has to consider the overlap in sensitivity of the methods applied to the properties. In addition, the successful derivation of a consistent rock physics framework transforms geophysical properties to the reservoir rock fluid description. This study demonstrates successful integration of seismic-and-CSEM-derived properties within a rock-physics framework.

The final results were obtained based on an integrated approach using regional geological knowledge, high-quality dual-sensor seismic, towed-streamer EM and well log data to achieve the best possible interpretation. We have shown that we can handle the challenge of complex background resistivities, image the embedded small thin reservoir, and discriminate reservoir fluids by combing the strengths of seismic and CSEM data through quantitative integration. The final product of the reservoir characterization process can estimate the total volume of hydrocarbon in place within a reservoir.

Acknowledgments

We would like to thank PGS for permission to publish this work. We would also like to thank Andrew Long, Vinnie Papenfus and Aoife O'Mongain for their input. We thank Scripps and the

Seafloor Electromagnetic Methods Consortium for developing MARE2DEM. Integrated products and services were provided under licence from Rock Solid Images Inc, to patent numbers US8064287, US7912649 and US12/135,729 and their related families.

Reference

Chen, J., and G. M. Hoversten [2012]. Joint inversion of marine seismic AVA and CSEM data using statistical rock physics and Markov random fields. *Geophysics*, **77**(01), R65–R80, doi: 10.1190/geo2011-0219.1.

Constable, S. C., R. L. Parker, and C. G. Constable [1987]. Occam’s inversion – A practical algorithm for generating smooth models from electromagnetic sounding data. *Geophysics*, **52**(03), 289–300.

Du, Z. & MacGregor, L. [2010]. Reservoir characterization from joint inversion of marine CSEM and seismic AVA data using the Genetic Algorithms: a case study based on the Luva gas field. *80th SEG Annual International Meeting 2010*, Expanded Abstract.

Du, Z and Hosseinzadeh, S. [2014]. Seismic guided EM inversion in complex geology: Application to the Bressay and Bentley heavy oil discoveries, North Sea. *75th EAGE Conference & Exhibition*, Expanded Abstract.

Figueiredo, L. P., D. Grana, M. Santos, W. Figueiredo, M. Roisenberg and G. S. Neto, [2017]. Bayesian seismic inversion based on rock-physics prior modeling for the joint estimation of acoustic impedance, porosity and lithofacies. *J. Comput. Phys.* **336**, 128-142, doi:10.1016/j.jcp.2017.02.013.

Gao, G., A. Abubakar, and T. M. Habashy [2012]. Joint petrophysical inversion of electromagnetic and full waveform seismic data. *Geophysics*, **77**(3), WA3–WA18, doi: 10.1190/geo2011-0157.1.

Harris, P., Du, Z., MacGregor, L., Olsen, Shu, R. and Cooper, R. [2009]. Joint interpretation of seismic and CSEM data using well log constraints: an example from the Luva Field. *First Break*, **27**, 73-81.

Key, K., and J. Ovall [2011]. A parallel goal-oriented adaptive finite element method for 2.5-D electromagnetic modelling. *Geophys J Int*, **186**(1), 137–154.

Key K., Du Z., Mattsson J., McKay, A. and Midgley, J. [2014]. Anisotropic 2.5D inversion of Towed Streamer EM data from three North Sea fields using parallel adaptive finite elements. *76th EAGE Annual Conference & Exhibition*, Extended Abstracts.

Løseth, L.O., Wiik, T., Olsen, P.A and Hansen, J.O. [2014]. Detecting Skrugard by CSEM – Prewell prediction and postwell evaluation. *Interpretation*, **2** (3), SH67–SH78.

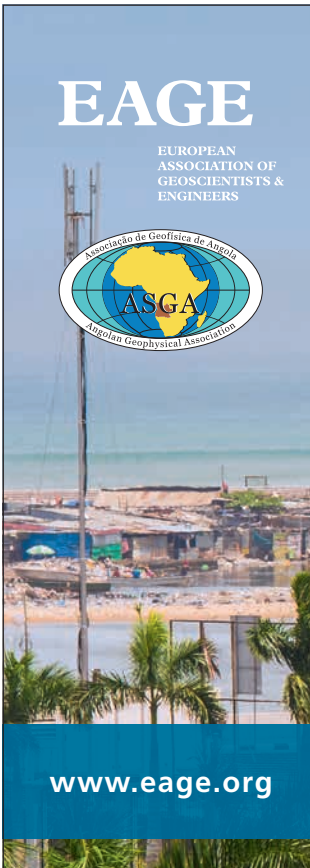
McKay, A., Mattsson, J. and Du, Z. [2015]. Towed Streamer EM – reliable recovery of sub-surface resistivity. *First Break*, **33**, 75-85.

Pedro, A., A. Alvarez, L. MacGregor, F. Bolivar, R. Keirstead and T. Martin [2017]. Reservoir properties prediction integrating controlled-source electromagnetic, prestack seismic, and well-log data using a rock-physics framework: Case study in the Hoop Area, Barents Sea, Norway. *Interpretation*, **5** (02), SE43-60, <http://dx.doi.org/10.1190/INT-2016-0097.1>.

Reiser, C., T. Bird and M. Whaley [2012]. Reservoir property estimation using only dual-sensor seismic data – a case study from the West of Shetlands, UKCS. *First Break*, **33**, 67-75.

ADVERTISEMENT





www.eage.org

First EAGE/ASGA Workshop on Petroleum Exploration

Challenges and Solutions for Deep Water Exploration in Angola

2-4 October 2017 – Luanda, Angola

EAGE and ASGA (Angolan Geophysical Association) have joined forces for the organization of the First EAGE/ASGA Workshop on Petroleum Exploration themed ‘Challenges and Solutions for Deep Water Exploration in Angola’. The aim will be to address some of the challenges faced by Angolan Deep water Explorers. The event is a golden opportunity for geoscientists to brain-storm over issues related to exploration offshore in West Africa,

The following topics will be discussed:

- New 4D Technology
- Advanced Seismic Acquisition
- AVO
- Operational Efficiency
- Deepwater & Ultra-deepwater Exploration Challenges & Solutions
- Pre-salt Exploration, Subsalt Imaging & CO2 Predictions
- Case Studies on Brazil Experience

Join us in Luanda for this highly topical workshop. For more information please visit the workshop eventpage.

Registration is now open!